

Adiabatic demagnetization refrigerators for small laboratory experiments and space astronomy

C. Hagmann and P.L. Richards

University of California, Department of Physics, Berkeley, CA 94720, USA

Received 29 November 1994

An overview is given of the general principles and techniques used for the design and construction of compact, portable adiabatic demagnetization refrigerators (ADRs). The paper covers methods of salt pill suspension, magnet technology, lead design, heat switches and temperature readouts, as well as considerations for space qualification. Performance specifications are given for an ADR which was originally developed for cooling infrared detectors on the Space Infrared Telescope Facility (SIRTF). This ADR is presently used on the balloon-borne Millimeter Wave Anisotropy Experiment (MAX) for measuring anisotropy in the cosmic microwave background. Comparisons are made with other ADRs under development for use in space or on rockets.

Keywords: adiabatic demagnetization; refrigerators; space cryogenics

Compact adiabatic demagnetization refrigerators (ADRs) are increasingly used for cooling small experiments to 50 mK. They are single shot devices but can have duty cycles of more than 95%. The cooling power is typically $1 \mu\text{W}$ at 100 mK, which is small compared with dilution refrigerators but adequate for many purposes. Operating temperatures as low as 50 mK are practical. Somewhat larger cooling powers are possible by increasing the overall size. Modern compact ADRs are simple, portable and relatively inexpensive. The operating temperature is easily varied by changing the magnetic field. Their ability to work in zero g has led to the development of prototypes for satellite applications.

ADRs are normally operated from a high temperature reservoir at $T \approx 1.5 \text{ K}$. Reservoir temperatures around 4 K, which can be provided by an unpumped liquid helium or bath or a mechanical refrigerator, require an additional stage of refrigeration, especially when long hold-times are required and large heat capacities are to be cooled. Compact ^3He refrigerators have been used for this purpose. A two-stage ADR is also a practical alternative. The other basic requirements for an ADR are a vacuum, a small superconducting magnet, a paramagnetic salt pill and a heat switch.

At present, ADRs are used in observational millimetre wave and X-ray astronomy and as testbeds for the development of detectors for millimetre waves, X-rays and dark matter. In this paper we will review the current status of compact ADR technology. We refer mostly to the ADR¹ developed at Berkeley originally as a prototype for the Space Infrared Telescope Facility (SIRTF), but not now

included in the plans for that spacecraft. However this ADR has flown on the Millimeter Wave Anisotropy Experiment (MAX) and has been duplicated in several laboratories for use in detector development. We will also provide some information on other projects including the ADR² under development at NASA Goddard Space Flight Center for the Advanced X-ray Astronomical Facility (AXAF) and the rocket-borne ADR developed at Wisconsin³. Similar ADRs have been developed at NASA Ames Research Center⁴ and at Princeton⁵. A schematic diagram of the SIRTF ADR is given in *Figure 1* and the parameters of the ADR are summarized in *Table 1*.

Refrigeration cycle

The ADR cycle is illustrated in *Figure 2* by reference to the entropy diagram of a typical paramagnetic salt. The cycle begins by closing the heat switch between the thermal reservoir and cold stage and ramping the magnetic field up to move along the line A→B. The magnetic moments of the salt are thereby aligned, the entropy of the moments is reduced, and the heat of magnetization is transferred to the reservoir. After a pause at point B, to achieve thermal equilibrium, the switch is opened and the field is adiabatically decreased. The lattice temperature of the salt falls as entropy is transferred from the lattice to the magnetic moments. The salt is partially demagnetized to some operating temperature T_f which is indicated by point C, after which the field is reduced isothermally along the line C→D to compensate for the heat leak. By regulating the magnetic field, a stable temperature can be maintained for

Table 1 Parameters of the SIRTf ADR

Amount of CCA	0.07 moles
Heat of magnetization	≈ 1 J
Time constant	1 s at 100 mK
Energy pumped at 100 mK	28 mJ
Conduction heat leak	$0.35 \mu\text{W}$
Hold time at 100 mK	23 h
Duty cycle	$>95\%$
Heat switch conductance	10 mW K^{-1} at $T=1.5$ K
Reservoir temperature	1.5 K
Mass of 100 mK stage	100 g
Resonant frequency	240 Hz
Mechanical Q	100
Total mass	5 kg

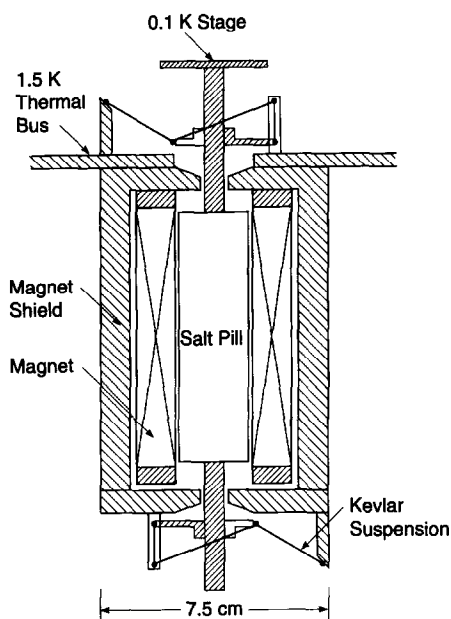


Figure 1 Schematic diagram of SIRTf ADR

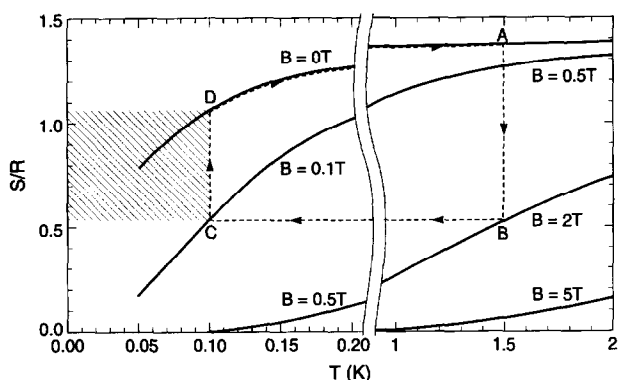


Figure 2 Temperature dependence of entropy of the paramagnet chromic caesium alum (CCA) for several values of applied magnetic field. The molar entropy is normalized to the ideal gas constant. The refrigeration cycle runs from A to D. The hatched area to the left represents the energy which the paramagnet can absorb at temperature T_i

many hours. Once point D is reached, the ADR must be cycled again.

Paramagnetic salt pill

We use the paramagnetic salts ferric ammonium alum (FAA) with $J = 5/2$ or chromic caesium alum (CCA) ($J =$

$3/2$) as our working substance. FAA has higher entropy density and more cooling power than CCA and is used in our balloon ADR as well as the AXAF and Wisconsin ADRs. We selected CCA⁶ for the SIRTf ADR because it can withstand higher bakeout temperatures than FAA. The salt is grown from solution on a mesh of gold wires and sealed in a stainless steel container to prevent loss of the water of hydration⁶. The wires are silver-soldered to an OFHC copper bolt which is used as the thermal bus to the 100 mK experimental stage. This pill design avoids materials that are attacked by the corrosive salt. It is very reliable, has a thermal time constant of ≈ 1 s at $T = 100$ mK and negligible eddy current dissipation. A full description of the considerations for selection of the paramagnetic salt for a single stage ADR and of the details of construction and testing is given in reference 6. Information about the choice of paramagnetic salt for a two-stage ADR is given in reference 7.

Magnet and shield

For space applications, it is important to minimize heat dissipation in the LHe bath. The heat input from the magnet current leads can be troublesome, but can be reduced by using a magnet with a high field-to-current ratio. For SIRTf, we use a superconducting solenoid (from Cryomagnetics, TN, USA) with a bore diameter of 2.5 cm, which produces a central field of 2.3 T at a current of 1.5 A. The magnet is conduction cooled and quench protected by built-in diodes. For less demanding laboratory or balloon applications, solenoids with $B/I \approx 0.4 \text{ T A}^{-1}$ are typical. They are less expensive and the winding volume is smaller.

The Wiedemann-Franz (WF) law⁸ states that the ratio of electronic thermal to electrical conductivity for any normal metal is $\kappa/\sigma = L_0 T$, where the Lorenz number $L_0 = 2.45 \times 10^{-8} \text{ W } \Omega \text{ K}^{-2}$. Consequently, resistive alloys or pure normal metals can be used as magnet leads with similar heat dissipation. Brass leads are often used, as they are less susceptible to thermal runaway than copper leads, whose resistance rises sharply with temperature. The cross-section to length ratio A/L of the leads can be chosen to minimize the heat dissipation over a refrigeration cycle. Given a 95% ADR duty cycle, a magnet current of 2 A and a heat sink temperature of $T = 77$ K, brass wires have an optimum $A/L \approx 2 \times 10^{-4} \text{ cm}$. The heat leak is then 3 mW at zero current and 50 mW at 2 A for each lead with 6 mW average dissipation.

The dissipation due to ohmic losses can be eliminated by using superconducting leads. We have tested commercially available high T_c superconducting leads (from ICI Superconductors, UK) between $T = 77$ K and $T = 4$ K. The leads consist of 2 mm diameter, 10 cm long yttria stabilized zirconia rods coated with $50 \mu\text{m}$ of $\text{YBa}_2\text{Cu}_3\text{O}_7$. The critical current at $T = 77$ K is 1 A, so a total of four rods is necessary for the SIRTf magnet. We measured a heat leak of 5 mW for each rod. Presumably this was dominated by the zirconia substrate. This technology is expected to improve.* In demanding applications, Nb_3Sn wires which have a critical current density $j_c \approx 10^5 \text{ A cm}^{-2}$ can be used from LHe

* For example, the ZerRes Corporation (Boston, MA, USA) has announced high temperature leads with heat leaks of $\approx 50 \text{ mW}/100 \text{ A}$ per pair

temperature to ≈ 12 K with high temperature superconducting materials continued to ≈ 77 K.

Another source of dissipation at LHe temperature is due to a.c. losses in the magnet as the current is ramped up and down. We estimated the a.c. losses in the low current SIRTf magnet by measuring $\int IV dt$ over a complete magnet cycle lasting 35 min. The upper limit on the heat input was 2 J, which gives an average dissipation of $30 \mu\text{W}$ for an ADR hold time of 20 h, which is small compared to the other losses.

A magnetic shield has been employed in some recent ADRs. It contains the magnetic flux and reduces the danger of large induced e.m.f.s ($V = d\Phi/dt$) during a magnet quench. Also, it decreases microphonic noise caused by vibrating leads and eliminates calibration errors in the thermometers caused by magnetoresistance effects. Several types of magnetic shields can be used. A passive ferromagnetic shield of vanadium permendur works well in fields up to about 3 T. It improves the field homogeneity, is usable with a simple solenoidal magnet, but contributes substantially to the weight of the ADR. In applications where induced e.m.f.s are of little concern, a thin shield can be used which is saturated at full field, but is effective in the much smaller field used for temperature regulation. Another choice is an active shield formed by a bucking coil in series with the central magnet. Such shields are relatively lightweight but have larger stray field. For a review of different shielding concepts used for ADRs see reference 9.

As shown in *Figure 1*, we use a ferromagnetic shield and flux return. The shield was designed by requiring that it returns all of the magnetic flux when saturated. With the shield in place it is a good approximation to assume that the field inside the magnet bore is uniform and longitudinal, and that it falls linearly with radius within the magnet windings. For example, to carry the flux in the symmetry plane perpendicular to the magnet axis we require that

$$\Phi_0 = B_0 \left(A + 2\pi \int_{r_1}^{r_2} r dr (r_2 - r) / (r_2 - r_1) \right) = B_s \pi (r_3^2 - r_2^2) \quad (1)$$

where A is the area of the magnet bore, r_1 and r_2 are the inner/outer winding radii, and r_3 is the outer radius of the shield. The above condition was used to select the thickness of the cylindrical walls and a similar argument determined the thickness of the end-plates. Here the condition at r_2 is

$$\Phi_0 = B_s 2\pi r_2 t \quad (2)$$

where t is the thickness of the end-cap. A more accurate check of the shield performance can be made by using the public domain computer program POISSON.* The SIRTf shield is made of vanadium permendur with a large saturation flux of $B_s \approx 2.3$ T at $T = 4$ K (reference 10). After fabrication the shield was annealed in high vacuum at 870°C for 8 h and furnace cooled at 250°C h^{-1} (reference 11). To reduce its thermal time constant, the shield was plated with 0.5 mm of copper. Field uniformity could be improved by using a higher saturation material such as holmium¹² for the central part of the end caps. A more com-

plete description of the design and testing of the magnetic shield for the SIRTf ADR is given in reference 1. The measured stray field outside of the shield was only a few gauss at full field and agreed well with the calculated values. With the measured quench time of 0.1 s, the e.m.f. generated in the worst case circuit around the equator of the shield is $\approx 10 \mu\text{V}$.

Quenches in modern magnets are unlikely but precautions must be taken to safely dissipate the energy released in such an event. The stored energy in the SIRTf magnet is ≈ 500 J at full current, which could be dumped into the superfluid LHe bath on the spacecraft through a high conductivity copper thermal strap. The computed temperature rise within the instrument chamber was 40 mK. In a two-stage ADR used with a mechanical refrigerator, the fields and stored energies (several kilojoules) are higher, while the total heat capacity is lower. A quench at full field in this case would cause considerable heating.

Heat switch

The requirements for the heat switch include a large on/off ratio of thermal conductance, reliability and small power dissipation. Mechanical heat switches¹³ give the best performance, but gas gap heat switches¹⁴ have also been used. The mechanical heat switch shown in *Figure 3* is based on a commercial linear solenoid with copper windings (Part 129450-035, Ledex Inc., OH, USA). A current of 100 mA closes the jaws on a cold finger which extends from the 100 mK stage and produces a force of 200 N. The cold finger and jaws are made of OFHC copper and gold plated to resist corrosion. Flexible copper braid bolted to the high temperature reservoir is soldered to each jaw. The thermal conductance of the switch at $T = 1.5$ K was measured to be 10 mW K^{-1} . We have used both copper and NbTi superconducting windings on the solenoid. The former allows closing the heat switch at liquid nitrogen temperature with a voltage of ≈ 15 V. This is useful during initial cooldown of the ADR to conserve liquid helium. The ohmic losses at $T = 1.5$ K of ≈ 30 mW might not be tolerated in satellite applications and a superconducting solenoid would then be preferred. A prototype superconducting switch very similar to that in *Figure 3* was built by Ball Aerospace as part of

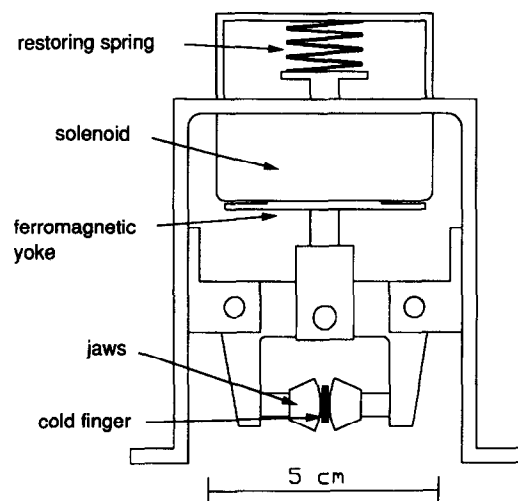


Figure 3 Mechanical heat switch in the SIRTf ADR. The lightweight frame is made of aluminium; the moving parts are of stainless steel

* Available from the POISSON Group, Los Alamos National Laboratory, Los Alamos, NM 87545, USA

the definition studies for SIRTf. It survived a vibration test at room temperature and was cold tested at Berkeley. The switch was cycled at helium temperature 10 000 times without loss in thermal conductance or noticeable wear. About 2000 cycles would be expected in a five year satellite mission.

Gas-gap heat switches rely on the thermal conductivity of helium contained between two surfaces. Activated charcoal adsorbs the ⁴He gas in the off condition. Because they are always closed for $T > 30$ K, initial cool-down of the ADR is facilitated. They have the disadvantage of a finite conductance in the off state due to conduction along the gas tight container. For a gas switch designed for AXAF, the power required to warm the charcoal to desorb the gas is 35 mW. The heat leak in the off state is $\approx 10 \mu\text{W}$ (reference 2) for a reservoir temperature of $T \approx 1.5$ K. This would be the dominant heat leak for small ADR systems. In order to obtain a useful hold time, the salt mass must be larger than the value in Table 1 with resulting increases in the weight and size of the ADR.

ADR suspension

The ADR hold time varies inversely with the heat load which is usually dominated by conduction along the mechanical supports. The suspension needs to be strong enough to raise the mechanical resonance frequency of the cold stage above typical driving frequencies. It should also lie well above any signal frequency to minimize microphonic noise. Modern ADRs have resonant frequencies of a few hundred hertz. For a fixed resonance frequency, the ADR hold time is roughly independent of salt pill size as long as the cold mass is dominated by the salt pill and the heat leak is dominated by the supports. This can be seen from the expression for resonant frequency, $\omega \propto (EA/Lm)^{1/2}$, where E is the Young's modulus, A is the support cross-section, L is the length and m is the cold stage mass. For a given temperature difference, the hold time t is proportional to the ratio of the mass of salt to the thermal conductance, $t \propto m_s L / \kappa' A$, where κ' is the average thermal conductivity. If m is dominated by the mass of the salt, then $t \propto E / \kappa' \omega^2$. For maximum hold time, the figure of merit for the suspension material is E / κ' . Here

$$\kappa' = 1 / (T_2 - T_1) \int_{T_1}^{T_2} \kappa(T) dT$$

is the thermal conductivity $\kappa(T)$ of the support material averaged over the temperature distribution. Commonly used materials include Kevlar 29 and Kevlar 49 (Du Pont Fibers, DE, USA), nylon and stainless steel. Table 2 lists the mechanical and thermal properties of suspension materials. Kevlar is the best available material and is used in several recent ADRs.

When designing a Kevlar suspension, care must be taken to ensure that the Kevlar remains tensioned when cooled. Kevlar expands by $\approx 0.1\%$ when cooled to liquid helium temperature¹⁵, while aluminium shrinks by $\approx 0.5\%$. Moreover, tensioned Kevlar 49 (29) yarn creeps¹⁶ at room temperature by 0.02 (0.05)% log₁₀ (number of hours under tension). For Kevlar 29 braid, the creep rate is about three times larger than that of yarn¹⁷. If tensioned to 25% of its breaking strength, which corresponds to 0.6% elongation

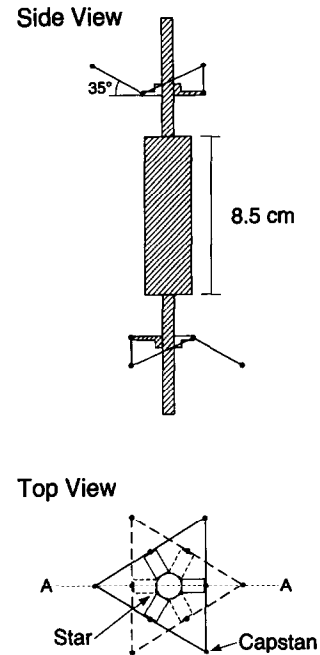


Figure 4 Kevlar suspension system of the SIRTf ADR. Dots represent miniature capstans for uniform tensioning. A single strand of Kevlar 29 cord is used on each end of the pill. Solid lines represent the top suspension system and dashed lines the bottom one

Table 2 Mechanical and thermal properties of suspension materials

Suspension material	Elastic modulus, E (GPa) ^a	Heat leak (μW) ^c
Kevlar 29 yarn ^b	62 ^d	19 $T^{2.1}(A/L)$
Kevlar 49 yarn	117 ^d	24 $T^{2.1}(A/L)$
Nylon	5.5 ^d	9 $T^{2.7}(A/L)^{29}$
NbTi	80 ³⁰	50 $T^3(A/L)^{31}$
Stainless steel	200 ³²	735 $T^2(A/L)^{29}$

^aElastic modulus E is given at 300 K, except for NbTi which is at 4 K

^bKevlar 29 is also available in the form of braids (woven fibres) with E about three times smaller than that of yarn (parallel fibres)

^cThe heat leak to 0.1 K from a reservoir at temperature T in the liquid helium range through a suspension with cross-section to length ratio A/L in cm is given by the integral

$$(A/L) \int_{0.1}^T \kappa(T') dT'$$

which is not sensitive to the low temperature limit. The heat leak for Kevlar was measured in this work

^dData from manufacturer

for Kevlar 49 and 1% for Kevlar 29 and stored at room temperature for one year, Kevlar would lose all tension upon cooling. The need for re-tensioning can be avoided at the cost of a small decrease in resonance frequency by adding a small metal spring in series with the Kevlar. The spring constants of the metal and the Kevlar should be comparable. The tension T can be checked by plucking the cords and measuring the vibration frequency $f = (T/\rho)^{1/2} / 2L$, where ρ is the mass per unit length.

Several techniques are available for terminating Kevlar. If used in the form of a braid, it can be wrapped around a smooth pulley or capstan and will be held in place by friction after tensioning. If used as yarn, the fibres can be epoxied through a hole in a metal fitting³. Figure 4 shows the

suspension of the SIRTf ADR. It uses braided cords of 25 kg breaking strength Kevlar 29 (from Cortland Cable, NY, USA) with cross-sectional area $A = 10^{-3} \text{ cm}^2$ and a total $A/L = 4 \times 10^{-3} \text{ cm}$. One cord on each end of the salt pill connects anchors on the warm heat sink to a star shaped aluminium cantilever spring attached to the pill. At each vertex, the cord makes one full turn around a 5 mm diameter capstan which is free to rotate to allow uniform tensioning. Each capstan is then locked in place to fix the location of the pill. The angle between the Kevlar cords and the symmetry plane is 35° in order to match the frequencies of the lowest frequency resonances. The complete set of calculated eigen-frequencies of the salt pill suspension system is given in Table 3. The fundamental resonance frequency of the suspension system, with a 100 g salt pill, was measured to be $\approx 240 \text{ Hz}$.

To demonstrate that this ADR can survive vibrations encountered in a rocket launch, a dummy model of the SIRTf ADR was vibration tested at room temperature and at $T = 77 \text{ K}$ at NASA Ames. Sinusoidal accelerations were applied at frequencies from 5 Hz to 1 kHz¹. At $T = 300 \text{ K}$, the fundamental resonance frequency was 240 Hz with a quality factor Q of 100 for small accelerations. It decreased to ≈ 10 at higher amplitudes. The test at $T = 77 \text{ K}$ gave almost identical results. The Kevlar broke when driven at the resonance frequency with an amplitude between 30 and 40 g, corresponding to $\approx 300\text{--}400 \text{ g}$ of acceleration of the dummy pill. The energy stored is $\approx m(\alpha g/\omega)^2$ for an acceleration equal to αg . Consequently, for a given Q , the energy dissipated per second $P = m(\alpha g)^2/\omega Q$. Since the Q values of low temperature metals are larger than that of Kevlar, this power heats the Kevlar. The temperature rise in the Kevlar is of the order of 100 K for $\alpha \approx 30$. This heating may account for the similarity of the results at 77 and 300 K and contribute to the failure of the suspension when driven at the resonant frequency.

If the spacecraft vibrations are represented by a power spectral density $w(f)$ which is flat over the resonance line-width, then the r.m.s. acceleration can be estimated using Miles' formula¹⁸

$$\langle a^2 \rangle = (\pi/2) Q f_0 w(f) = (\alpha g)^2 \quad (3)$$

Using the SIRTf parameters from above, $\alpha \approx 30$ for $w(f) = 0.05 \text{ g}^2 \text{ Hz}^{-1}$ which is typical for a Titan 4 rocket spectrum around 200 Hz. Several approaches can be used to relax these stringent requirements on the salt pill suspension set by launch vibrations. A mechanical filter can be placed between the spacecraft structure and the ADR to reduce the value of $w(f)$ near the resonance frequency. It is also possible to clamp the salt pill with a mechanical heat switch, but at some risk of sticking due to cold welding.

Table 3 Calculated eigen-frequencies of the mechanical system shown in Figure 4 (the mass is assumed to be uniformly distributed, and the salt pill radius and length are represented by r and l , respectively)

Mode direction	K_{eff}	m_{eff}	$\omega^2 (\theta = 35^\circ)$
z	$12 EA \sin^2 \theta/L$	m	$4 EA/mL$
x, y	$6 EA \cos^2 \theta/L$	m	$4 EA/mL$
θ_z	$12 EA r^2 \cos^2 \theta/L$	$mr^2/2$	$16 EA/mL$
θ_x, θ_y	$6 EA \cos^2 \theta (l/2)^2/L$	$ml^2/12$	$12 EA/mL$

Magnetic damping

As an alternative method for damping salt pill vibrations, we considered using a magnetic damper on the SIRTf ADR. The design is similar to a loudspeaker with a single turn short-circuited voice coil. A copper cup is attached to the free end of the salt pill and is placed in the air gap of the magnet as shown in Figure 5. For axial motion, the eddy current dissipation in the cup is given by

$$P_{\text{loss}} = \sigma v^2 B^2 V \quad (4)$$

where σ is the electrical conductivity of the cup, v is the velocity perpendicular to the magnetic field and V is the cup volume in the magnetic field B . The formula is valid as long as the electromagnetic penetration depth is large compared with the thickness of the cup. The damping term $\gamma = \omega_0 m/Q$ in the one-dimensional equation of motion

$$m d^2x/dt^2 + \gamma dx/dt + m \omega_0^2 x = F \quad (5)$$

is replaced by $\gamma \rightarrow \gamma + \sigma B^2 V$. For $1/\sigma = 10^{-10} \Omega \text{ m}$, $B = 0.5 \text{ T}$ and $V = 3 \times 10^{-8} \text{ m}^3$, γ is increased by a factor of 30. Due to mode coupling, it is adequate to damp one mode only. The conductivity σ given is estimated for OFHC copper at $T = 4 \text{ K}$. Due to dissipation in the damper, the copper will be heated and the damping will decrease slowly with time.

Electrical connections

The electrical leads for detectors and thermometers on the cold stage must have low thermal conductance. Furthermore, low microphonic noise is usually required for high impedance transducers. A sufficiently small thermal heat leak can be obtained by using thin wires of Pt-W, Manganin or NbTi with a typical diameter of 25–50 μm . When the capacitance to ground C of a wire, which is biased with a potential V , varies with time due to motion, the voltage induced across a transducer of resistance R is $RVdC/dt$. Several methods exist for reducing this noise. In one the wires are held fixed under tension by miniature leaf springs³. At Berkeley we use a stripline or ribbon cable. It is made by sandwiching the wires between two layers of adhesive Kap-

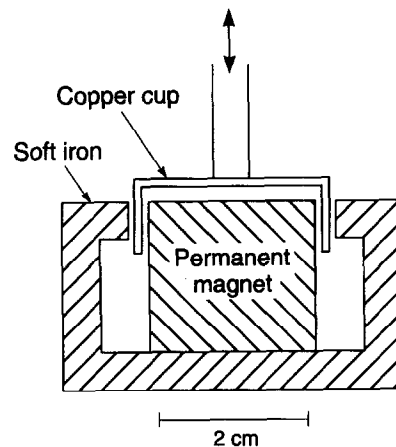


Figure 5 Schematic diagram of magnetic damper. The permanent magnet is made of Alnico 5 or Sm-Co and produces a field of $\approx 1 \text{ T}$ in the air gap. Vertical motion causes circular eddy currents which heat the copper cup

ton tape (Permacell 221, Fraylock Inc., CA, USA) thus fixing the relative positions of the wires but allowing flexibility between the cold stage and the reservoir. The capacitance of the signal wires to ground is kept constant and cross-talk is reduced by alternating ground wires with signal wires in the stripline. To minimize inductive pick-up, the loop areas should be made small by small spacings between adjacent wires.

Another promising technology uses thin lithographed metal traces on a Kapton substrate. Candidates for the metal include a superconductor such as Nb, a high resistance alloy, or even a high conductivity metal such as gold or copper. In the last case the metal must be thin (≈ 5000 nm) and narrow ($w \approx 0.5$ mm). The electron mean free path is then limited by thickness¹⁹ and is almost independent of temperature. The electronic thermal conductance of these traces can be estimated by measuring their electrical resistance and using the W-F law. One side of the Kapton can be fully metallized and serve as a ground plane, and the opposite side carries the traces which are fabricated with photolithographic techniques. Table 4 lists integrated thermal conductivities for various stripline materials. It is convenient to terminate the stripline with connectors. We employ miniature connectors (Part NSM25S2-LO5, Ulti Mate, Inc., CA, USA) with a pin spacing of 0.6 mm. The ends of the stripline are epoxied to a short sections of fibreglass circuit board which are also epoxied (using Stycast 2850FT, Emerson and Cummings, MA, USA) to the connector shell and the wires are soldered to the pins.

The SIRTf ADR uses a stripline with 25 Pt-W leads, 50 μm in diameter and 10 cm long and spaced by 0.6 mm. The Kapton has $A/L \approx 2.5 \times 10^{-3}$ cm, and the total stripline heat leak is $\approx 0.14 \mu\text{W}$ for a helium plate temperature of 1.5 K. The Kapton and adhesive contribute 0.13 μW . This could be further reduced by decreasing the wire spacing and/or increasing the length.

Temperature readout and regulation

The temperature of the ADR cold stage is read out with a calibrated germanium resistance thermometer (GRT). The same thermometer is also used for temperature regulation of the ADR during isothermal demagnetization. A stable ADR operating temperature reduces $1/f$ noise in bolometric detectors and it keeps the responsivity constant.

Standard precautions of low temperature thermometry must be used. Because of the large thermal boundary resistance, the bias power dissipated in the germanium thermometer needs to be small to reduce self heating of the chip. At $T = 0.1$ K, a power of 10^{-12} W typically produces

Table 4 Heat leaks of various stripline materials in the LHe range

Stripline material	Heat leak (μW) ^b
NbTi ³¹	$50 T^3 (A/L)$
Pt-W ³³	$(320 T^2 + 22 T^3) (A/L)$
Au	$0.015 T^2 (w/L)$
Kapton	$22 T^2 (A/L)$

^aFor Au a thickness t of 4000 nm was assumed and only the electronic contribution to the conductivity is given, as derived from the W-F law. For this thickness, we measured a 30% decrease in R upon cooling to $T = 4$ K

^bValues of A , L and W are in cm

a $\Delta T \approx 1$ mK. Therefore, low noise readouts are required. Initially we used a commercial GRT (Part GR-200A-30, Lake Shore Cryotronics, OH, USA) and an a.c. resistance bridge (Part AVS-46, RV-Elektronikka, Vantaa, Finland). The temperature readout noise was $\approx 5 \mu\text{K}$ for a time constant of 1 s. This system proved to be sensitive to pick-up and heating from electrical interference. An improved system based on bolometer readout technology^{20,21} used a neutron transmutation doped (NTD) germanium chip thermometer²². The thermometer is current biased at ≈ 100 Hz with a cold load resistor and read out by a cold differential JFET (from Infrared Labs, AZ, USA) located on the LHe plate and heated to ≈ 120 K. For NTD-19 with $N_A - N_D = 5.5 \times 10^{16} \text{ cm}^{-3}$, $d(\ln R)/dT \approx 50$, which is about five times larger than for the commercial GRT. We obtained a temperature noise of $\approx 0.5 \mu\text{K}$ and the system was less sensitive to pick-up.

The temperature regulation system²³ controls the magnet current by feeding back on the temperature readout. The error signal drives a proportional-differential (PD) filter and regulates the ramp rate of the magnet current. Digital²³ and more compact analogue versions of the PD circuit were built. The analogue controller has been used to successfully cycle the refrigerator and operate it by remote control during a balloon flight²⁴.

Thermal performance

A useful figure of merit of an ADR is Q_c/Q_i , where Q_c is the measured heat pumped in one cycle and $Q_i = T_f \Delta S$ is the theoretical pumped heat from the hatched area in Figure 2. The efficiency is less than one for several reasons: 1, thermal gradients along the salt and the thermal bus during demagnetization; 2, eddy current heating of the salt pill during demagnetization; and 3, entropy lost in cooling parts of the salt pill and other components. The first two effects can be minimized by careful design of the salt pill and thermal bus⁶. The last effect, occasionally called 'thermal ballast', can be calculated as

$$\Delta S_b = \int_{T_i}^{T_f} (C/T) dT$$

where C is the heat capacity of the addenda. For copper²⁵ in the LHe temperature range, the specific heat is $c(T) = (11T + 1.4T^3) \mu\text{J}^{-1} \text{g}^{-1} \text{K}^{-1}$, for pure aluminium²⁶ the value is $c(T) = (50T + 0.92T^3) \mu\text{J} \text{g}^{-1} \text{K}^{-1}$ for $T > T_c = 1.16$ K and $c(T) = 410 e^{-1.55/T} \mu\text{J} \text{g}^{-1} \text{K}^{-1}$ below T_c , and for stainless steel²⁷ $c(T) = (465T + 0.56T^2) \mu\text{J} \text{g}^{-1} \text{K}^{-1}$. In the SIRTf ADR, thermal ballast causes a loss in efficiency of a few per cent and the overall efficiency is estimated to be $\approx 90\%$. Cooling the photometer used in the MAX experiment²⁴ required $\approx 15\%$ of the heat pumped with a pill containing 0.08 moles of FAA.

The hold time of the ADR at temperature T_f is given by Q_c/P , where P is the average heat input into the cold stage, caused by conduction, radiation and vibration. Often thermal conduction dominates. A useful way of extending the hold time is to use a low temperature thermal intercept on the suspension and leads. This is typically done with a miniature charcoal pumped ³He or ⁴He refrigerator²⁸ with a still temperature of 0.3 or 0.8 K. On our balloon-borne ADR, such an intercept was used as a buffer between the

100 mK stage and the He bath, which could not be pumped during launch. A ^3He or ^4He fridge could be used to precool the salt pill before demagnetization and thus reduce the required magnetic field, but at the cost of a second heat switch and a longer cycle time.

Depending on the type of cryostat used, radiation heating of the salt pill and addenda can be significant. These parts must be surrounded by a radiation shield at or below 4 K. A significant area of the inside of the shield should be coated with infrared absorbing black paint to heat sink the radiation field. A millimetre thick layer of the black Stycast 2850FT has adequate absorptivity and good adhesion.

Vibrational heating can be very serious. If it is predictable and of short duration, one can reduce its effect on hold time by magnetizing the salt and maintaining it at temperature T during the vibration. The increase in entropy due to vibration is then reduced by T_v/T . This was done for the MAX balloon launch.

Acknowledgements

This paper summarizes work done by a large number of people. Especially valuable contributions were made by P. Timbie, G. Bernstein, A. Clapp and W. Holmes. This work was supported by NASA grants FD-NAGW-2121 and NAGW-2864.

References

- 1 Timbie, P.T., Bernstein, G.M. and Richards, P.L. Development of an adiabatic demagnetization refrigerator for SIRTF *Cryogenics* (1990) **30** 271–275
- 2 Serlemitsos, A., SanSebastian, M. and Kunes, E. Design of a spaceworthy adiabatic demagnetization refrigerator *Cryogenics* (1992) **32** 1431–1437
- 3 McCammon, D. Personal communication, University of Wisconsin (1993)
- 4 Savage, M.L., Kittel, P. and Roellig, T. Salt materials testing for a spacecraft adiabatic demagnetization refrigerator *Adv Cryog Eng* (1990) **35** 1439–1446
- 5 Ruhl, J. and Dragovan, M. A portable 0.050 K refrigerator for astrophysical observations *Proc 4th Int Workshop on Low Temperature Detectors for Neutrinos and Dark Matter* (Eds Booth, N.E. and Salmon, G.L.) Edition Frontiers, Gif sur Yvette, France (1991) 461–464
- 6 Hagmann, C., Benford, D.J. and Richards, P.L. Paramagnetic salt pill design for magnetic refrigerators used in space applications *Cryogenics* (1994) **34** 213–219
- 7 Hagmann, C. and Richards, P.L. Two-stage magnetic refrigerator for astronomical applications with reservoir temperatures above 4 K *Cryogenics* (1994) **34**, 221–226
- 8 Kittel, C. *Introduction to Solid State Physics* 6th Edn, Wiley, New York, USA (1986)
- 9 Warner, B.A., Shirron, P.J., Castles, S.H. and Serlemitsos, A.T.

- Magnetic shielding for a spaceborne adiabatic demagnetization refrigerator (ADR) *Adv Cryog Eng* (1992) **37B** 907–914
- 10 Ackermann, F.W., Klawitter, W.A. and Drautman, J.J. Magnetic properties of commercial soft magnetic alloys at cryogenic temperatures *Adv Cryog Eng* (1971) **16** 46–50
- 11 Josso, E. Iron-cobalt-vanadium alloys: A critical study of the phase diagrams in relation to magnetic properties *IEEE Trans Magn* (1974) **MAG-10**(2) 161–165
- 12 Schauer, W. and Arendt, F. Field enhancement in superconducting solenoids by holmium flux concentrators *Cryogenics* (1983) **23** 562–564
- 13 Siegwarth, J.D. A high conductance helium temperature heat switch *Cryogenics* (1976) **16** 73–76
- 14 Torre, J.P. and Chanin, G. Heat switch for liquid helium temperatures *Rev Sci Instrum* (1984) **55** 213–215
- 15 Hartwig, G. and Knaak, S. Fibre-epoxy composites at low temperatures *Cryogenics* (1984) **24** 639–647
- 16 Horn, M.H., Riewald, P.G. and Zwieben, C.H. Strength and durability characteristics of ropes and cables from Kevlar aramid fibers *Proc Oceans '77: Third Annual Combined Conf MTS and IEEE* New York, USA (1977) 24E1–24E12
- 17 Duband, L., Hui, L. and Lange, A. Thermal isolation of large loads at low temperature using Kevlar rope *Cryogenics* (1993) **33** 643–647
- 18 Harris, C. and Crede, C. (Eds) *Shock and Vibration Handbook* 2nd Edn, McGraw-Hill, New York, USA (1976) 24–28
- 19 Fuchs, K. The conductivity of thin metallic films according to the electron theory of metals *Proc Camb Phil Soc* (1938) **34** 100–108
- 20 Kittel, P. Ultimate temperature stability of a magnetic refrigerator *Cryogenics* (1983) **23** 477–478
- 21 Devlin, M., Lange, A.E., Wilbanks, T. and Sato, S. A d.c.-coupled high sensitivity bolometric detector system for the infrared telescope in space *IEEE Trans Nucl Sci* (1993) **40** 162–165
- 22 Haller, E.E. Physics and design of advanced IR bolometers and photometers *Infrared Physics* (1985) **25** 257–266
- 23 Bernstein, G., Labov, S., Landis, D., Madden, N. *et al.* Automated temperature regulation system for adiabatic demagnetization refrigerators *Cryogenics* (1991) **31** 99–101
- 24 Devlin, M.J., Clapp, A.C., Gundersen, J.O., Hagmann, C.A. *et al.* Measurements of anisotropy in the cosmic microwave background radiation at 0.5 degree angular scales near the star gamma ursa minoris *Ap J* (1994) **430** L1–L4
- 25 Schutz, R.J. Thermal relaxation calorimetry below 1 K *Rev Sci Instrum* (1974) **45** 548–551
- 26 Phillips, N.E. Heat capacity of aluminum between 0.1 K and 4.0 K *Phys Rev* (1959) **114**(3) 676–685
- 27 Hagmann, C. and Richards, P.L. Specific heat of stainless steel below $T = 1$ K *Cryogenics* in press
- 28 Duband, L., Hui, L. and Lange, A. A space-borne ^3He refrigerator *Cryogenics* (1990) **30** 263–270
- 29 Lounasmaa, O.V. *Experimental Principles and Methods Below 1 K* Academic Press, London, UK (1974) 17–54
- 30 Easton, D.S. and Koch, C.C. Mechanical properties of superconducting Nb-Ti composites *Adv Cryog Eng* (1977) **22** 453–462
- 31 Olson, J.R. Thermal conductivity of some common cryostat materials between 0.05 and 2 K *Cryogenics* (1993) **33** 729–731
- 32 *Metals Handbook* 8th Edn, American Society for Metals, Metals Park, OH, USA (1961)
- 33 Buhl, A.J. and Giauque, W.F. Use of platinum alloy for electrical leads at liquid helium temperatures: heat conductivity *Rev Sci Instrum* (1965) **36** 703